Detection of periodic motion trajectories: Effects of frequency and radius

Frances Wilkinson Centre for Vision Research, York University, Toronto, Ontario, Canada

Yousra Haque Centre for Vision Research, York University, Toronto, Ontario, Canada

Psychological Sciences Research Institute & Institute of Neuroscience, University of Louvain, Louvain-la-Neuve, Belgium

Charles C.-F. Or Centre for Vision Research, York University, Toronto, Ontario, Canada

Audrey S. Gottlieb Centre for Vision Research, York University, Toronto, Ontario, Canada

Hugh R. Wilson Centre for Vision Research, York University, Toronto, Ontario, Canada

Periodic trajectories are an important component of biological motion. Or, Thabet, Wilkinson, and Wilson (2011) studied radial frequency (RF) motion trajectory detection and concluded that, for RF2–5 trajectories, the threshold function paralleled that of static RF patterns. We have extended Or et al.'s (2011) findings to a broader range of RFs (three to 24 cycles) and across a 4-fold range of radii (1°–4°). We report that (a) thresholds for RF trajectories decrease as a power function of RF for low RF trajectories (three to six cycles) before approaching an asymptote at high RFs (12–24 cycles); (b) detection thresholds for RF trajectories scale proportionally with radius; and (c) there is no lower versus upper field advantage in the parafoveal field for stimuli displaced from fixation on the vertical midline. The results are compared to earlier findings for static RF thresholds, and we argue that our findings support the existence of parallel spatial and temporal processing channels that may contribute to both action perception and production.

Introduction

Curvature is a fundamental property of the natural visual world, defining the shapes of a wide range of natural objects including many animals and plants. In the laboratory, closed quasi-circular contours have been successfully used to explore the intermediate stages of shape processing in both psychophysical and imaging studies. This line of investigation was inspired by the electrophysiological work of Gallant, Braun, and Van Essen (1993) and Gallant, Connor, Rakshit, Lewis, and Van Essen (1996) who demonstrated that concentric and radial grating stimuli elicit stronger responses from macaques V4 neurons than parallel Cartesian gratings, suggesting a specialization for such patterns at intermediate stages of form processing. More recent functional magnetic resonance imaging (fMRI) observations of human V4 using concentric stimuli have reinforced this finding (Dumoulin & Hess, 2007; Wilkinson et al., 2000).

One class of pattern that has proved particularly useful in studying visual shape analysis is radial frequency (RF) patterns (Wilkinson, Wilson, & Habak, 1998). Defined as closed contours deviating from circularity by sinusoidal modulation of the radius in polar coordinates, RF patterns of various RFs, amplitudes, and phases can be combined to resemble the bounding contours of curved real-world objects while maintaining mathematical tractability (Wilson &

Citation: Wilkinson, F., Haque, Y., Or, C. C.-F., Gottlieb, A. S., & Wilson, H. R. (2016). Detection of periodic motion trajectories: Effects of frequency and radius. *Journal of Vision, 16*(7):10, 1–15, doi:10.1167/16.7.10.

doi: 10.1167/16.7.10 Received September 27, 2015; published May 16, 2016 ISSN 1534-7362

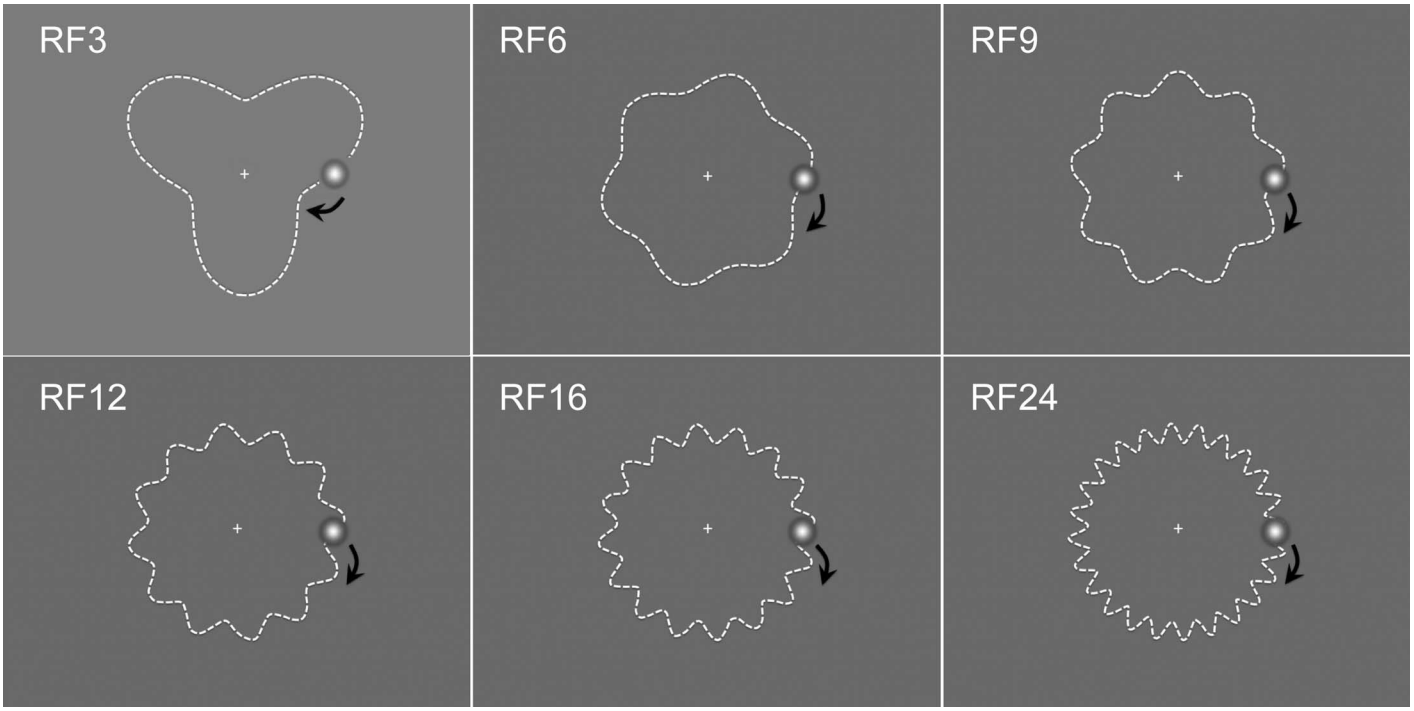

Figure 1. RF-defined motion stimuli: RF3, RF6, RF9, RF12, RF16, and RF24. The dashed lines represent RF trajectories that were not visible but were to be extracted from path of the DOG target. Phase angle (ϕ) was 0° for all trajectories in Experiments 1 and 2. All trajectories began to the right of the fixation point as indicated by the position of the DOG in each panel above, and movement was in the clockwise direction.

Wilkinson, 2002). Thresholds for discriminating RF modulated patterns from circles decrease as a function of increasing RF over the range from one to five cycles, flattening out to an asymptotic level for high RFs. For patterns of small radius, asymptotic sensitivity is in the hyperacuity range; the minimum detectable displacement from circularity on the retina is less than the diameter of a cone (Westheimer, 1979). Global pooling of local orientation and curvature information underlies the extreme sensitivity to deformation at low RFs (Hess, Wang, & Dakin, 1999; Jeffrey, Wang, & Birch, 2002; Loffler, Wilson, & Wilkinson, 2003); at higher RFs, however, thresholds depend increasingly on probability summation and less on global pooling (Jeffrey et al., 2002; Loffler et al., 2003).

While less obvious than its contribution to the shape of natural objects, curvature is also an important feature of motion paths in the natural world. The extensive literature on biological motion demonstrates that we are exquisitely sensitive to the trajectories traced by key joints in the body as a human or other animal moves through space (see Blake & Shiffrar, 2007, for review; Johansson, 1973), and a great deal of gestural communication depends on an accurate reading of such trajectories. Trajectories that smoothly change direction and speed along curved paths are generally indicative of biological motion in the natural world, and the kinematic control of such movements has been the focus of decades of research. Only recently, however, with the discovery of the mirror neuron system has emphasis been placed on making the link between the production of movement and the perception of movement trajectories (Rizzolatti et al., 1996; Rizzolatti & Sinigaglia, 2010).

Just as complex spatial forms represent a hierarchy of simpler components, the analysis of which may be mapped onto successive levels of the ventral visual pathway (Wilson & Wilkinson, 2014, 2015), the recognition of complex patterns of movements such as the actions of a "point-light walker" (Johansson, 1973) requires the integration of many local component motions, each of which describes the motion of some local part contributing to the articulated whole. Recently we have begun exploring parallels between intermediate levels of form and motion perception by introducing a motion analogue to static RF patterns—RF trajectories. In our initial study, Or, Thabet, Wilkinson, and Wilson (2011) measured detection thresholds for motion-defined RF2–RF5 target trajectories. Contours were never visible in their entirety and detection was based solely on shape extracted by following the trajectory of a moving target (Figure 1, upper left panel illustrates an RF3 trajectory). Several parallels with the static RF findings emerged. Thresholds decreased as a power function of increasing RF; however, motion trajectory thresholds were up to 6 times higher than those reported previously for corre-

sponding static patterns (Wilkinson et al., 1998). Strong evidence of global pooling across cycles of the trajectory was found, and a subsequent study (Daar, Or, & Wilson, 2012) revealed a dipper function in RF trajectory increment thresholds, analogous to that seen in the contrast domain (Nachmias & Sansbury, 1974) and for RF discrimination functions using static RF patterns (Bell, Wilkinson, Wilson, Loffler, & Badcock, 2009). Recent fMRI studies with RF motion trajectories have implicated cortical areas V2 and V3 in the early analysis of these stimuli, and show selective activation of several higher level form and motion areas as well (Gorbet, Wilkinson, & Wilson, 2012, 2014).

Although Or et al.'s (2011) RF trajectory thresholds paralleled previous static RF results, their stimuli were limited to a low RF range (two to five cycles). They did not explore the domain of high RF analysis, where local processing has been shown to dominate in spatial studies (Jeffrey et al., 2002; Loffler et al., 2003; Wilkinson et al., 1998). The aim of the present study was to extend Or et al.'s (2011) findings to higher RFs by measuring the detection thresholds of RF6–RF24 trajectories. Secondly, we examined the effect of pattern radius on detection thresholds across a 4-fold range of radii, asking whether the shape constancy at threshold (equivalent Weber fractions) reported for static RF patterns (Wilkinson et al., 1998) would also be seen for trajectory detection. Our results indicate that parallels between static RF patterns and motion RF trajectories extend to high RF analysis. Finally, motivated by the subjective reports of observers in the main study, we carried out a follow-up experiment comparing RF sensitivity in upper and lower visual fields.

Methods

Observers

A total of 17 individuals aged 20–58 years participated in the experiments reported here. All had normal or corrected-to-normal visual acuity, and all testing was binocular. The study protocol was approved by the York University Human Participants Review Committee and conformed to the guidelines of the Helsinki Declaration. Written informed consent was obtained from each observer before the experiment. Specific details about observers are reported below for each study.

Stimuli

The stimuli were RF trajectories defined by the path of a circularly symmetric target moving around a central fixation point. The target had a difference of Gaussians (DOG) luminance profile:

$$\mathrm{DOG}(R) = 1.8\exp\left(\frac{-R^2}{\sigma^2}\right) - 0.8\exp\left(\frac{-R^2}{(1.5\sigma)^2}\right) \quad (1)$$

where R is target radius from its center and σ was 7.1′. The peak spatial frequency and bandwidth were 2.74 cpd and 1.79 octaves at half-amplitude. The contrast was held constant at 100%.

RF trajectories (Or et al., 2011) are the temporal analogue to spatial RF patterns (Wilkinson et al., 1998). As shown in Figure 1, the target DOG follows a circular path, the radius of which is modulated sinusoidally in polar coordinates over time:

$$r(vt) = r_0[1 + A\sin(\omega vt + \phi)] \quad (2)$$

where the target's polar location r is a function of mean radius r_0, radial sinusoidally modulated amplitude A, RF ω, angular speed v, time t, and phase angle of trajectory ϕ. Radial amplitude of 0 produces a perfect circular trajectory; this trajectory was the comparison stimulus in the discrimination task described below. The phase angle (ϕ) determines the rotation of the shape described by the trajectory. In each experiment reported here, a single phase angle was used. The core data reported by Or et al. (2011) for low RF trajectories followed the same approach. In a control condition in the same paper, Or et al. reported that randomizing the phase of RF3 trajectories did not elevate thresholds compared to testing with a single phase, and that thresholds for the four phases tested did not differ statistically from one another.

The trajectories (dotted lines in Figure 1) were to be extracted by attending to the DOG target while maintaining fixation on a small central cross. In each interval, the DOG traveled one complete revolution in the clockwise direction, describing either a perfect circle or an RF trajectory. Details of frame rates will be discussed in the individual experiments below; all were chosen to create the percept of smooth motion.

A brief note is in order to clarify the way in which speed is defined in this report. The target always moved at a polar angular speed v of 180°/s, completing a full trajectory in 2 s. The tangential speed at which the target is moving along a unit distance in the visual field depends on the radius of the trajectory path. These unit trajectory distances are converted to visual angles and the tangential speeds reported in terms of visual angle in degrees per second. So for a circular trajectory subtending a radius of 1° at our viewing distance of 114 cm, the full length of the trajectory covered by the target in 2 s was 6.28°, so we describe its tangential speed as 3.14°/s. This tangential speed is also the average speed for the RF trajectories; however, the modulation of their radii introduces slight variations in

instantaneous speed as the target traverses the peaks and troughs of the RF path. Near threshold these variations are very small, and in a control experiment in which instantaneous speed along the trajectory path was held constant (i.e., angular speed varied slightly) Or et al. (2011) demonstrated that it is the deviations from the circular path rather than the small variations in speed that underlie performance on this task.

Apparatus

The stimuli were presented on an eMac computer, with a refresh rate of 112 Hz, spatial resolution of 800×600 pixels, and grayscale of 8 bits/pixel. The mean luminance, measured with a Minolta LS-100 photometer (Konica Minolta Sensing Americas, Inc., Ramsey, NJ), was 79 cd/m^2 after gamma correction. In a dimly lit room, observers used a chin and forehead rest to maintain a viewing distance of 114 cm. The screen subtended a visual angle of $15.7° \times 11.8°$, forming square pixel width of 1.18′. Custom software written in MATLAB 7.4 (The MathWorks, Inc., Natick, MA) using the Psychophysics Toolbox (Brainard, 1997) was used.

General procedure

Data were collected using a two-alternative temporal forced choice paradigm and the method of constant stimuli. One temporal interval contained the RF target trajectory and the other (order determined randomly) contained a circular trajectory of radius equal to the mean radius of the target. Observers were instructed to maintain fixation on a central cross throughout each trial. For each trial, the fixation cross appeared 500 ms before the onset of the first trajectory and remained visible throughout the trial. The two trajectory intervals were separated by a 1500-ms interstimulus interval. The task of the observer was to indicate by a keyboard response which of the two intervals (1 or 2) contained the RF trajectory. Auditory feedback (beep) was provided in Experiments 1 and 2 for incorrect responses.

Each experimental run consisted of 10 trials of a single RF at each of five or six amplitude levels, and took approximately 7 min to complete. Observers were told which RF trajectory would be presented at the beginning of each run. For each RF tested, six runs were conducted, yielding a total of 60 trials at each amplitude. Runs of different RFs were interleaved in randomized order. Testing was split over several sessions at the convenience of the observers. Prior to beginning threshold assessment, pilot runs were conducted with each observer at each RF to provide experience with the task and to determine a suitable range of amplitudes for threshold determination.

For each observer and RF condition, data were combined over sessions. The percentage of correct trials at each amplitude was calculated; a Quick (1974) or Weibull (1951) function was fit to the data, and the 75% threshold was determined by interpolation. An estimate of standard deviation was computed by bootstrapping.

Experiment 1: Trajectory thresholds as a function of radial frequency

Observers

Eight individuals participated in Experiment 1. Seven of the observers, including author YH, were experienced psychophysical observers, five of whom had also participated in the studies reported by Or et al. (2011). Two observers (one experienced, one novice) were naive as to the purpose of the study.

Procedure

Observers' detection thresholds were measured for RFs of three, six, nine, and 12 cycles (see Figure 1) in interleaved blocks as described in General procedure. The mean radius of the RF trajectories (r_0 in Equation 2) was held constant at 1°. Each stimulus was drawn using 57 frames (four screen refreshes/frame), visible for 35.7 ms at angular intervals of 6.43° with the final frame overlapping the initial frame.

Results and discussion

Individual thresholds of the eight observers are plotted in Figure 2. Thresholds decrease as a function of increasing RF and are well fit by straight lines on a log–log plot; the exponents of least squares fits to the individual data range from −0.84 to −1.15 (mean −0.97) indicating a power-law relationship.

In Figure 3, red circles represent the mean thresholds averaged across all eight observers; note that all calculations and statistical analyses were carried out on log threshold values. Also plotted (blue triangles) are the mean scores from Or et al. (2011) for the comparable condition (constant angular speed 3.14°/s). It is evident that the two data sets are very similar in the range of overlap in RF; this is not surprising as five individuals participated in both studies. It is also clear that the slope of the function is flattening with increasing RF (mean slope = −1.5 over the range of two to five cycles from Or et al. [2011], and −0.97 over the range of three to 12 cycles tested here). This suggests

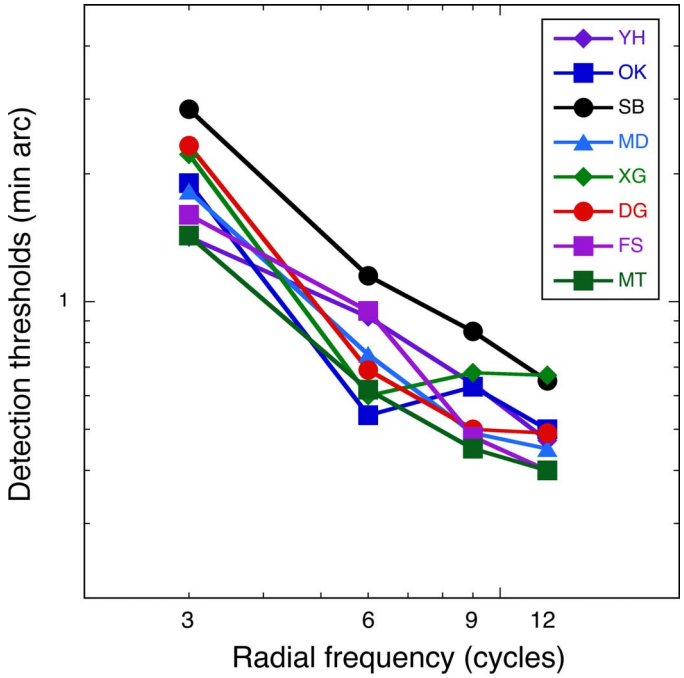

Figure 2. Trajectory detection thresholds plotted against radial frequency for eight observers in Experiment 1.

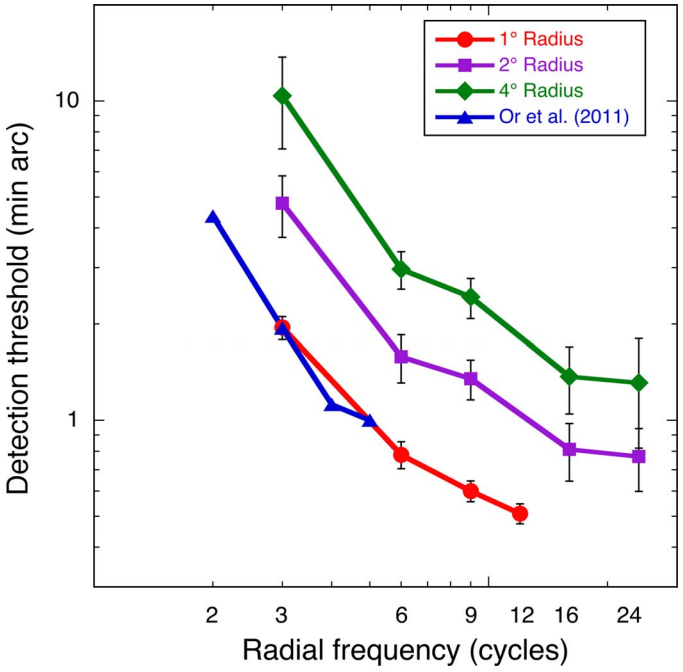

Figure 3. Average thresholds from Experiment 1 (red circles) and from Or et al. (2011; blue triangles) for the same stimulus radius and velocity plotted against RF. Also shown are results from Experiment 2 for RF trajectories with larger radii (2°: purple squares; 4°: green diamonds). Error bars = 1 *SE*.

that thresholds may asymptote at higher RFs. However, a paired t test reveals that there was a statistically significant difference between thresholds for RF9 and RF12 trajectories, $t(7) = 3.95$, $p = 0.006$, indicating that an asymptotic level had not been reached by RF9. Testing of higher frequency trajectories was not possible with a 1° radius because the size of the target was too large relative to the periodicity of the modulations to resolve the trajectory patterns.

Among other properties seen for static RF patterns (Wilkinson et al., 1998) was a scaling of thresholds with radius. Thresholds expressed as Weber fractions (proportion of the radius) were found to be comparable over a range of four octaves. In Experiment 2, we examine whether RF trajectories show a similar scaling with increasing radius. Furthermore, with larger radii, we were able to extend the range of trajectory frequencies tested to ask whether asymptotic performance would occur at higher RFs.

Experiment 2: Trajectory thresholds as a function of pattern radius

Observers

A total of 10 observers, including authors YH and AG, participated in Experiment 2; five were experienced psychophysical observers, of whom four had participated in Experiment 1 and the remaining five were naive. All had normal or corrected-to-normal vision and were tested binocularly.

Procedure

Observers' detection thresholds were measured as a function of the mean radius of the trajectory patterns (r_0). Three radii (1°, 2°, 4°) were tested in interleaved blocks, each containing five to six levels of amplitude modulation. (Experienced observers who had participated in Experiment 1 with 1° radii were tested with 2° and 4° radius patterns only). Observers were assigned one of three RFs (RF3, RF6, or RF9) with the exception of observer YH, who was tested at all frequencies. Five observers (one naive) were also tested using higher RF trajectories (RF16 and RF24): two with 2° radius, two with 4° radius, and one (YH) at both radii.

Increasing the trajectory radius introduced some jerkiness to the appearance of the DOG motion. To minimize this, we decreased the number of screen refreshes per frame to two and doubled the number of frames per trajectory to 114. The angular speed remained constant at 180°/s but each frame's angular rotation and duration were thus halved (to 3.19° and 17.7 ms), creating the perception of smooth motion. A

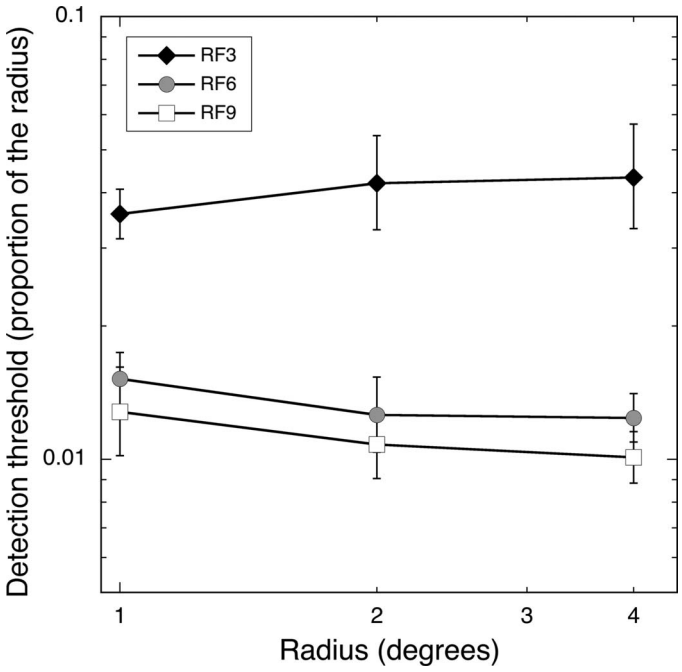

Figure 4. Trajectory detection thresholds expressed as proportions of the radius (Weber fractions) for groups of participants tested with RF3 ($N = 4$), RF6 ($N = 4$), or RF9 ($N = 3$) trajectories at each of three radii (1°, 2°, and 4°). Error bars = 1 *SE*.

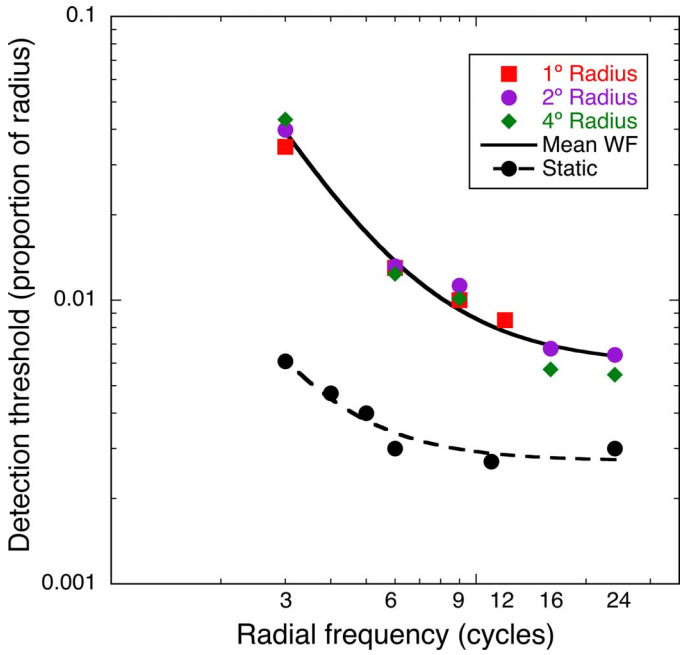

Figure 5. Mean thresholds (Weber fractions) at three radii plotted against RF. Black circles are thresholds for static RF patterns from previous studies (Bell, Badcock, Wilson, & Wilkinson, 2007; Bell et al., 2009; Loffler et al., 2003; Wilkinson et al., 1998). The solid curve is fit to the mean Weber fraction calculated at each RF. The dashed line is the same fit to the static RF thresholds.

pilot study on experienced observers showed no differences between RF trajectories at the two different frame rates.

Results and discussion

Data for the 2° (purple circles) and 4° (green diamonds) radii are plotted with the data from Experiment 1 in Figure 3. Scaling the radius produced a near proportionate increase in detection thresholds across patterns of $r_0 = 1°$, 2°, and 4°; when the radius was doubled, the threshold also increased by a factor of approximately 2. While the curves in Figure 3 represent data collected from all observers, not all of whom were tested on all three radii, the scaling effect was also very clear in the thresholds of individual observers (five experienced, four naive) who were tested at all three radii using a single RF (Figure 4). The thresholds for these observers, converted to Weber fractions (proportion of the radius) were compared in a two-way mixed-model ANOVA with radius as the repeated measure and RF as the between-groups factor. As predicted from Experiment 1, the effect of trajectory frequency was significant, $F(2, 8) = 7.53$, $p = 0.014$; thresholds were highest at the lowest frequency (RF3) and decreased with increasing RF. However, neither the within-subjects factor of radius nor the interaction between radius and RF reached statistical significance (radius: $F(1.14, 9.12) = 0.053$; $p = 0.853$; interaction: $F(2.29, 9.12) = 1.262$, $p = 0.334$; Greenhouse–Geisser correction applied).

As described in Experiment 1, the slope of the threshold function for 1° radius patterns appeared to decrease with increasing RF. With the larger radii, it was possible to expand the range of RF trajectories to include RF16 and RF24. As is evident in Figure 3, performance approached an asymptotic level at these higher RFs. In Figure 5, the thresholds from Figure 3 have been converted to Weber fractions (proportion of the radius). It is clear that the three functions superimpose almost perfectly, as would be expected if threshold scales with radius. To model the reduction in threshold as a function of RF, we fit a decaying power function with an asymptote to the average of the Weber fractions at each RF:

$$T = a \cdot \omega^{-b} + c \quad (3)$$

where T is the trajectory threshold, a the weight factor, ω the RF, b the exponent, and c the asymptote.

This function (solid line in Figure 5) predicts an asymptotic level of 0.0059. When the same function was fit separately to the data for each of the three radii (c.f. Figure 3), it predicted asymptotic threshold levels of 0.44′, 0.75′, and 1.3′ for 1°, 2°, and 4° radii, respectively.

For purposes of comparison, black circles in Figure 5 are thresholds (Weber fractions) for static RF patterns drawn from the literature (Bell, Badcock, Wilson, & Wilkinson, 2007; Bell et al., 2009; Loffler et al., 2003; Wilkinson et al., 1998) and fit with the same function. For static patterns, the predicted asymptotic Weber fraction (0.0027) was about half of that predicted for RF trajectories.

Thus we have confirmed that RF trajectories show two properties previously described for static RF patterns. Firstly, thresholds scale as a function of radius. In the case of static RF patterns, scaling was seen over a four-octave range (0.25°–4°); for dynamic patterns we have limited our investigation to the 1°–4° range. Secondly, thresholds decline steeply (power law function) over the lower RF range (two to six) but gradually level off approaching an asymptotic value at RFs above approximately 12 cycles. It should also be noted that in terms of absolute thresholds, sensitivity is approximately 6–8 times greater for static patterns at very low RFs (Or et al., 2011), but this difference is reduced to a factor of 2 at asymptote.

Experiment 3: Upper and lower visual fields

Previous literature has examined functional specializations within the visual field in terms of central versus peripheral, left versus right, and upper versus lower visual fields (see Karim & Kojima, 2010, for review). The final experiment in this study was motivated by subjective reports by some of our observers suggesting that their judgments had been most influenced by movements in the lower visual field. Previous studies have reported an advantage for the lower visual field in terms of actions in near space such as arm movements (Danckert & Goodale, 2001; Khan & Lawrence, 2005) and visual anticipation of trajectory paths (representational momentum task; Gottwald, Lawrence, Hayes, & Khan, 2015). Since the stimuli in Experiments 1 and 2 were always centered at fixation and always moved clockwise into the lower field first, one explanation of the observers' impression of a lower field advantage is that this is a primacy effect; however, it seemed worthwhile to investigate this further, asking whether any threshold differences would be revealed if the trajectory stimuli were confined to the upper or lower visual fields. We examined this using two RFs, one (RF4) from the low frequency portion of the function in Figure 3 and the other (RF9) from the portion of the function at which asymptotic threshold values are approached.

Observers

Eight individuals (aged 21–58 years) with normal or corrected-to-normal vision participated in this study. Five also participated in Experiments 1 and/or 2, including authors YH and AG. The remaining three had not participated in prior studies with RF trajectories and were naive as to the underlying hypothesis of Experiment 3.

Stimuli and apparatus

The stimuli were similar to those described in Experiments 1 and 2; however, they were generated on a different display system using different software. For the present study, stimuli were generated using VPixx™ v2.62 software (VPixx Technologies, St-Bruno, QC, Canada) and displayed on a Samsung SyncMaster 900NF™ display with a screen resolution of 1024×768 pixels and a 120 Hz refresh rate (Samsung Electronics Canada, Inc., Mississauga, ON, Canada). At the viewing distance of 114 cm, the display subtended a visual angle of $17.3° \times 13.0°$.

Circular and RF trajectories with mean radii of 2° were centered 3.5° above or below a central fixation cross. As in the previous experiments, the trajectory was described by the movement of a target with a difference of circular Gaussians ($\sigma = 7.1'$) luminance profile at 100% contrast. The tangential speed of the target was 6.28°/s, and the phase angle (ϕ) of all trajectories was 90°. This created a vertically symmetric diamond-shaped trajectory for RF4. The initial position of the target was 1.5° above or below the fixation cross, which was the closest point in the trajectory to the fixation point. Target motion was always clockwise. Thus upper field stimuli moved up and to the left from their starting position, and lower field stimuli moved down and to the right.

Procedure

A two-interval forced-choice paradigm was used with the method of constant stimuli to assess thresholds for RF trajectory detection in the upper and lower fields. Observers were instructed to maintain fixation on the fixation cross throughout each trial, and trajectories presented in the two intervals of a single trial were at the same location (i.e., both upper field or both lower field). Within an experimental run, upper field and lower field trials were randomly intermixed, and four trials at each of five or six displacement amplitudes were presented in each field. Sessions with RF4 and RF9 stimuli were randomly interleaved, and data were cumulated over runs to achieve a total of at

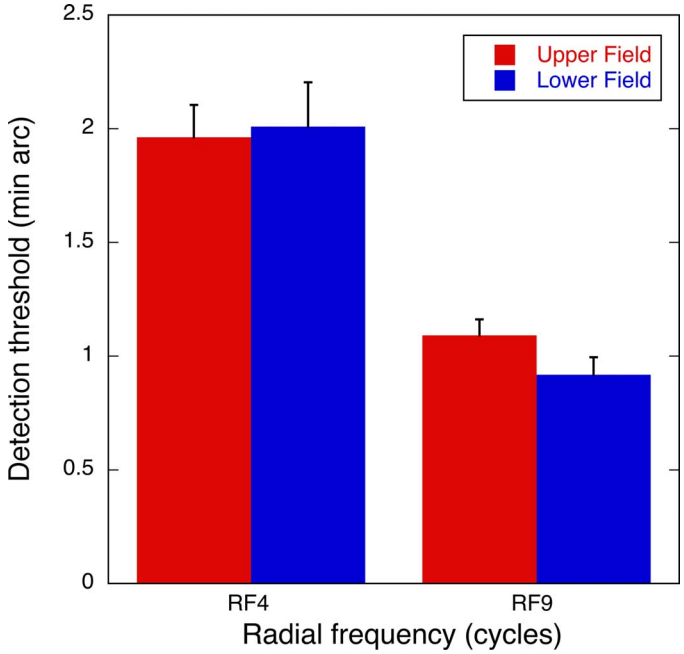

Figure 6. Average upper and lower field thresholds for detecting RF4 and RF9 trajectories. Error bars = 1 *SE*.

least 32 trials at each amplitude/visual field/RF combination.

Two observers (YH, LL) were also tested with the same 2° radius patterns centered at fixation (foveal control condition) to allow a direct comparison across the two experimental set-ups.

In response to questions raised by reviewers about the possible contribution of screen persistence (visual streaks), the same two observers were retested with foveally centered 2°-radius RF4 and RF9 trajectories with DOG target contrast reduced to 40%; foveal tests were also conducted with target speed reduced by a factor of two such that a single closed trajectory took 4 s to complete. Both these manipulations should reduce the strength of visual streak stimulation. Finally, the same two participants were retested foveally with phase of the same RF4 trajectory randomized across trials. This produces trajectories that are diamond-like ($\phi =$ 90°), square-like ($\phi = 270°$), and tilted in either direction between the two ($\phi = 0°$ or 180°). RF9 trajectories were not tested as phase shifts in high RF stimuli are tiny and so do not convey different shapes as they may for low RF trajectories.

Results

The foveal control condition yielded threshold deformation amplitudes for RF4 of 2.1′ (LL) and 1.9′ (YH), and for RF9 of 1.3′ (LL) and 1.1′ (YH). These values are comparable to those measured in Experiment 2 for 2° radius trajectories in our other experimental setup, indicating that differences in hardware and software did not affect our results. Decreasing the contrast of the target to 40% did not significantly alter performance, as would have been predicted if slight screen persistence had provided explicit orientation or curvature cues in the original high contrast condition. (LL: thresholds lowered by 5%–16%; YH: thresholds elevated by 9%–23%). Similarly, reducing the speed of the dot movement improved (lowered) thresholds for LL (RF4 and RF9) and for YH (RF4); only one threshold (YH: RF9) was elevated slightly (10%). Finally, thresholds averaged across the four test phases were comparable to our original RF4 single-phase baselines (LL: 2.1′ vs. 2.1′; YH: 1.8′ vs. 1.9′).

Thresholds measured in the upper and lower visual field are shown in Figure 6. A threshold could not be determined for one observer (XG) in one condition (RF9 upper field) due to extreme variability in his data, so the statistical analysis that follows is based on the remaining seven observers.

The 2×2 repeated measures ANOVA revealed a significant main effect of RF trajectories, $F(1, 6) = 55.60$, $p < 0.001$; as expected from Experiment 1, thresholds were lower for RF9 than for RF4 trajectories. However, neither the main effect of visual field, $F(1, 6) = 0.726$, $p = 0.43$, nor the interaction effect between the two factors, $F(1, 6) = 0.415$, $p = 0.54$, reached statistical significance. Thus contrary to the subjective impressions of some of the observers, the lower visual field does not show an advantage on this task.

Discussion

The results of the foveal measurements increase our confidence that RF trajectory analysis is indeed based on comparison of trajectories based on sequential motion signals rather than on a sequential activation of the same local orientation and curvature mechanisms thought to underlie static RF pattern analysis. If screen persistence produced low-contrast oriented line segments determining our thresholds at 100% target contrast, the visibility of such segments should be greatly reduced at 40% target contrast; similarly, reducing the speed of target motion by 50% should reduce the length of such local virtual line segments detectable at any instant. Since we are measuring the limit of sensitivity to deviations of the trajectory from a circular path, we would have expected either of these manipulations to substantially elevate thresholds if persistence were involved. This did not happen. Another nonmotion cue, which could conceivably underlie performance on our task, would be an accumulation of dot position information relative to the fixation point (i.e., slight changes in this separation

distance, which is constant for the circular trajectory, might be the critical indicator of the RF trajectory). Two findings from the literature make this highly unlikely. Or et al. (2011) carried out a control for their RF3 trajectory threshold measurements in which participants were instructed to track the target with their eyes, with no fixation point present. This did not elevate thresholds compared either to the central fixation condition used by Or et al. and in the present study, or to tracking with the fixation cross still present (and hence providing a separation marker) but not fixated. Moreover, Wilson and Fung (2016) have recently reported that when RF3 or RF4 trajectories are split into cycles and the cycles presented in random order rather than as a continuous trajectory, thresholds are elevated by at least a factor of 2 despite the fact that no position information was lost. Therefore, we are confident that RF trajectory detection is a distinct, motion-based problem.

Turning to the comparison of upper versus lower field performance, it is noteworthy that not only were thresholds equivalent for trajectories centered at ±3.5° vertical eccentricity; these thresholds were also not elevated compared to those measured in the foveal control condition. This probably reflects the fact that there is extensive overlap in the region of the visual field traversed by the target DOG for trajectories centered at fixation or at ±3.5°. A full examination of peripheral sensitivity either along the vertical or the horizontal meridian is beyond the scope of this study.

General discussion

The present study has extended the findings of Or et al. (2011) by showing that the pattern of sensitivity to RF trajectories is similar to that of static RF patterns in two respects. First, whereas at low RFs, sensitivity increases as a function of frequency, at higher RFs threshold sensitivity levels off, approaching an asymptote by 12 radial cycles. Second, sensitivity to the RF deformation of a circular trajectory scales with trajectory radius. Finally, despite the subjective impressions of observers of a reliance on the lower visual field in extracting RF motion cues, our psychophysical evidence does not support a lower field advantage in detecting either low RF (four cycles) or high RF (nine cycles) trajectories.

Motion versus static RFs: Similarities and differences

Since their introduction (Wilkinson et al., 1998), static RF patterns have been used by a variety of laboratories as a tool for quantifying shape sensitivity and discrimination. This work has revealed evidence of global spatial pooling as an intermediate stage in static form processing (Hess, Wang, & Dakin, 1999; Jeffrey et al., 2002; Loffler et al., 2003), and data from masking studies has suggested the existence of form-contour channels that in some ways parallel the contrast channels studied earlier using sine wave gratings and other spatially periodic stimuli (Bell & Badcock, 2009; Bell et al., 2009; Habak, Wilkinson, & Wilson, 2006).The present findings, in conjunction with other recent studies (Daar et al., 2012; Or et al., 2011), indicate very clear parallels between sensitivity to spatially and temporally defined deviations from circularity, although there are also differences. In the following we consider these similarities and differences in detail and ask to what extent these may indicate overlapping neural circuitry or homologous neural mechanisms that have been adapted to different purposes.

Shape of the threshold function

As illustrated in Figure 5, both the trajectory thresholds from the present study and the static thresholds drawn from previous work are well fit by power functions that approach an asymptote. The functions differ, however, in that the slope of the descending portion of the function is steeper for trajectory thresholds and the asymptotic values higher by a factor of 2.3. For the smallest radius (1°) used in this and previous RF trajectory studies, the asymptotic threshold amplitude is in the range of 25 arcsec; for static RF patterns of the same radius, this value is 11 arcsec. In view of the demands on short-term memory as trajectory information is cumulated over time (2 s in the present studies), this level of sensitivity is quite remarkable.

Threshold scaling with radius

Sensitivity for static RF patterns has been shown to scale across a range of radii from 0.25°–4°. Thus while the detection thresholds expressed as visual angles increased with radius, the same threshold amplitudes expressed as a proportion of the radius (Weber fractions) were constant across this range. As a consequence, these patterns exhibit shape constancy at threshold. The same result was found for trajectory thresholds in the present study for radii of 1°–4°. Therefore, thresholds expressed as Weber fractions allow us to generalize across a range of pattern or trajectory radii. We have argued elsewhere that this provides a valuable scalable spatial code for shapes (Wilkinson et al., 1998). The similar scaling reported here for trajectories is reminiscent of the findings of Jolicoeur and Ingleton (1991) showing scale invariance

in a curve-tracing task, and may reflect an important link between the perception and production of movement, a point we will return to later in this discussion.

Sensitivity in the upper and lower visual field

We undertook Experiment 3 only as a response to participant feedback that some felt they saw the deviations from circularity more definitively in the lower part of the trajectory around the foveal fixation point than in the upper portion; as such, our interest was in the immediate parafoveal region through which our stimuli had passed. The results of Experiment 3 clearly showed no difference between thresholds measured just above versus just below fixation (centered at 3.5°). At the time our study was conducted, there was no information in the literature about sensitivity differences across the visual field for static RF patterns, with the exception of a single published paper (Achtman, Hess, & Wang, 2000) and an abstract from our own laboratory (Wilkinson, Habak, & Wilson, 1997), both of which had looked only at scaling in the periphery along the horizontal meridian. Thus unlike the first two experiments, Experiment 3 was not designed as a comparison to preexisting static RF data. However, a reviewer drew our attention to the very recent work of Schmidtmann, Logan, Kennedy, Gordon, and Loffler (2015), which examined sensitivity to low frequency RF patterns at 5° and 10° eccentricity in the upper and lower as well as the left and right visual fields. These authors report that RF patterns, but not simpler orientation and curvature stimuli, produced lower thresholds in the lower visual field than at comparable lateral or upper field locations. For technical reasons, our paradigm and experimental setup could not be adapted to test these field locations. However, we did examine thresholds in a modified procedure in two participants, and found very little evidence of a comparable asymmetry for trajectory thresholds. In view of the fact that the existing literature on upper/lower field functional asymmetries has pointed to lower field superiority on some measures relating vision to action (Danckert & Goodale, 2001; Khan & Lawrence, 2005), this is clearly a question that deserves a full investigation, which is well beyond the scope of the current study.

Mechanisms supporting low and high RF thresholds

A number of studies have documented clear differences in performance for low frequency (two to five cycles) versus high frequency (10 cycles and above) static RF patterns (Bell et al., 2007; Jeffrey et al., 2002; Wilkinson et al., 1998). Minimum deformation thresholds for discriminating these patterns from perfect circles improve with increasing RF over the one to five cycle range. Over this range, strong evidence of global pooling operating across all cycles of the patterns has been confirmed by several laboratories, although differing underlying mechanisms have been proposed (Hess, Wang, & Dakin, 1999; Jeffrey et al., 2002; Loffler et al., 2003; Poirier & Wilson, 2006). By RF 10–12 cycles, thresholds were determined based on local features or pooling over only a small number of cycles (Jeffrey et al., 2002; Loffler et al., 2003). In the intermediate zone (five to 10 cycles), a combination of these mechanisms has been suggested to be operative. Or et al. (2011) showed a similar picture for temporally defined RF trajectories at low RFs, except that the slope of threshold decline is steeper, at least for the particular stimulus conditions replicated here.

Trajectory speed is one factor that might contribute to the poorer performances at low RFs and hence to the steeper slope of the trajectory function. While Or et al. (2011) did not find a statistically significant effect of speed over the range of angular velocities they examined (3.14°/s –12.57°/s), they did see a trend toward better performance at very low RFs (two cycles) as target speed increased, whereas thresholds for all speeds tested converged by RF5 (the highest frequency tested). The present study used only the lowest of the three speeds from the Or et al. (2011) study, and closely replicated the threshold values over this range. Thus we cannot rule out the possibility that there is a maximum time over which information about each cycle of the pattern can be accumulated without performance decrement and that this time is well under 1 s.

Another distinction made in earlier work on static RF patterns was that not only could shapes defined by low RFs be discriminated from circles at threshold, but at higher amplitudes, the individual shapes could be identified (Wilkinson et al., 1998). This was not the case for RF patterns above six cycles. Or et al. (2011) showed a similar ability to identify low RF trajectories (RF2–RF5). In these studies, the task was to indicate the number of cycles of deformation a stimulus pattern/trajectory contained from among four to six possible choices. In a recent fMRI study, Gorbet et al. (2014) reported that participants performed at chance on a behavioral discrimination between RF9 and RF10 trajectories when asked to choose the trajectory with the higher frequency, a task which should be less demanding than actually identifying the precise number of radial cycles. Performance with comparable static RF discrimination averaged 74% correct, suggesting static patterns may be ranked in terms of "bumpiness" even though they cannot be identified based on their shape, but even this does not seem possible for RF trajectories, at least not for nearest neighbors.

Thus the present findings add to the strength of the analogy between spatial and temporal stimulation by these periodically modulated polar stimuli. But does

this analogy have any functional significance? Could it be the case, for instance, that our RF motion stimuli somehow provide a weak but adequate signal to higher level form encoding mechanisms in the ventral visual pathway? Or is it the case that neural mechanisms in other parts of the brain specialized for motion analysis and, in particular, for the analysis of motion trajectories, have developed along similar principles to the spatial pathways?

Form from motion

There has been a great deal of interest in recent years in the convergence of motion and form information in the brain (e.g., Or, Khuu, & Hayes, 2007, 2010; reviewed in Kourtzi, Krekelberg, & van Wezel, 2008). Movement provides a rich source of information about the shape of an object: edge location and three-dimensional shape information are extracted from motion boundaries and motion gradients (Grill-Spector, Kourtzi, & Kanwisher, 2001; Murray, Olshausen, & Woods, 2003). Complex moving patterns of dots elicit strong percepts of articulated biological forms in motion (Johansson, 1973); brain areas in the superior temporal sulcus have been strongly implicated in biological motion analysis (Blake & Shiffrar, 2007; Grossman & Blake, 2002; Oram & Perrett, 1994). And the paths traced by moving objects or their parts can often be described in terms of shape; trajectories provide a contour description in time.

Neural representation of RF trajectories

The neural representation of RF trajectories was examined by Gorbet et al. (2012, 2014) using fMRI. RF trajectories gave rise to larger BOLD signals than did the analogous static RF pattern in all the topographically organized early cortical visual areas (V1, V2, V3, V3A, and V4), and in motion areas MT and STS (Gorbet et al., 2012). While there are difficulties equating the strength of motion and static patterns in terms of visibility time, degree of resulting adaptation, etc., it is difficult to imagine this result arising if the response to the motion trajectories reflected a weaker, degraded activation of the static analysis substrate, for example through "visual streak" activation of the same orientation-tuned neurons (Geisler, 1999; Geisler, Albrecht, Crane, & Stern, 2001). Furthermore, using multivoxel pattern analysis Gorbet et al. (2014) reported that classification accuracy for RF4 versus RF5 and RF9 versus RF10 was statistically significant for areas V2, V3, and MT, whereas none of the comparable comparisons between static RFs reached significance. So at these early levels of cortical analysis at least, distinct spatiotemporally tuned mechanisms appear to encode the local components of the trajectories, most probably curvature signals in V2 and combinations of local curvature signals in higher areas.

It is, however, possible that these distinct low-level form and motion signals still feed into common higher level analysis mechanisms, either through pathways traditionally thought to support cue-independent shape perception or through pathways more involved in planning motor acts and using object shapes to guide action. Relative to baseline responses, both static RF patterns and RF trajectories have been found to activate a wide range of dorsal and ventral visual areas as well as regions in the frontal lobes of the brain. Areas showing significantly greater responsiveness to low (discriminable) RFs than to high (nondiscriminable) RFs are much more limited, and convergence of such differential responding for both static and trajectory RFs was found in just two regions, one in the occipital-temporal region and one in the posterior parietal cortex (Gorbet et al., 2014).

The occipito-temporal activation occurred bilaterally in the region between motion-sensitive region MT and the lateral occipital area, an area which has been strongly implicated in cue-independent shape and object recognition (Grill-Spector et al., 2001; Kourtzi & Kanwisher, 2000; Vinberg & Grill-Spector, 2008).

The second zone of overlap, also seen bilaterally, was in the posterior parietal cortex in the inferior parietal lobule (IPL). This target area of the dorsal visual stream has been implicated in the "mirror neuron system," which supports the mapping of the visually observed actions of others onto the motor planning substrate for the same actions in the observer (Jastorff, Begliomini, Fabbri-Destro, Rizzolatti, & Orban, 2010; Rizzolatti et al., 1996; Rizzolatti & Sinigaglia, 2010), as will be described more fully below. However, IPL has also been implicated in the processing of global form in Glass patterns (Lestou, Lam, Humphreys, Kourtzi, & Humphreys, 2014) and may be part of a circuit that acts in concert with the ventral visual pathway to provide global integration of form.

Convergence in fMRI does not, of course, prove that pattern and trajectory analysis share the same neural circuits, only that the same general regions of the brain participate in some aspect of interpreting both types of input. Given the similarities demonstrated psychophysically in the present study and the previous study by Or et al. (2011) across a wide range of RFs and pattern/trajectory sizes, a valuable future step would be to look for direct evidence of pathway convergence. In earlier work, we delineated spatial zones of interaction for static RF patterns using masking (Habak, Wilkinson, Zakher, & Wilson, 2004), and investigated channels for RF shapes using adaptation (Bell et al., 2009). Similar approaches could be used to test for

interactions between spatial and temporal input signals of a single RF by, for example, measuring trajectory thresholds before and following adaptation to the equivalent static RF pattern or measuring static RF detection thresholds in the presence of a dot describing a high amplitude trajectory of the same frequency. Neural signatures for any psychophysically defined interactions could then be sought in these areas of convergence. Whether or not such investigations support the existence of shared mechanisms, future studies could also apply the methodologies used in earlier static RF studies (Bell & Badcock, 2009; Bell et al., 2007; Bell et al., 2009) to ask whether frequency-tuned RF motion channels underlie trajectory shape detection and discrimination.

Gorbet et al.'s (2014) fMRI analysis pointed to further brain regions of possible importance in discriminating among RF trajectories: the dorsal and ventral premotor cortex. These areas also showed stronger activation by the pair of trajectories that could be differentiated behaviorally (RF4 vs. RF5) than by the pair that could not be discriminated (RF9 vs. RF10). Unlike IPL, these regions were not activated by the analogous static RF patterns. Both IPL and ventral premotor cortex form part of the "mirror-neuron" system (Jastorff et al., 2010; Rizzolatti et al., 1996; Rizzolatti & Sinigaglia, 2010) involved in both the observation and execution of actions.

The involvement of both these areas in trajectory analysis strongly suggests that trajectory perception may play an important role in action planning as well as in action perception. RF trajectories entail repeated changes in curvature with accompanying decelerations and accelerations along a smoothly varying course. This sort of pattern is not seen in the movement of most inanimate objects which, when propelled into motion, follow a straight or parabolic course until a point of collision either terminates motion or occasions an abrupt change of direction. We do, however, see this sort of trajectory in the motion of articulated body parts as an animal or person moves through space, or makes goal-directed or gestural movements. We also see it in complex learned motor skills such as handwriting (Lacquaniti, Terzuolo, & Viviani, 1983; Viviani & Terzuolo, 1982). Movement identification and imitation depend both on encoding the functional goal of the movement, and its detailed trajectory, tasks which have been suggested to be the specific function of the parietal and premotor parts of this circuitry respectively (Lestou, Pollick, & Kourtzi, 2008).

One of the most extensively studied phenomena in the field of motor control is the "2/3 power law." This refers to the observation that curved biological movements show an inverse relationship between curvature and velocity; in the simplest case, when tracing or drawing ellipses, hand movements are slowest around the most strongly curved segments and fastest along the straight portions of the path. The 2/3 power law turns out to be ubiquitous for curved biological movements, describing movements as diverse as the body's center of mass and the swing of the foot during gait, smooth pursuit eye movements, and speech movements (see Dayan et al., 2007, for recent summary). Moreover, in terms of perception, trajectories that follow this relationship appear natural (i.e., biological; Bidet-Ildeil, Orliaguet, Sokolov, & Pavlova, 2006) and more surprisingly, give rise to the illusion of motion at a constant speed (Levit-Binnun, Schechtman, & Flash, 2006; Viviani & Stucchi, 1989), so our perception and production of movements is tightly linked. While our work to date with RF motion trajectories has almost exclusively examined near-threshold stimuli, we have noted in another recent study (Wilson & Fung, 2016) that as the amplitude of RF trajectories is increased (as in the examples shown in Figure 1) for a given angular velocity, they show a similar tangential velocity–curvature relationship. A recent fMRI study (Dayan et al., 2007) comparing activation by elliptical trajectories of dot arrays that conform to the 2/3 power law versus arrays that violate this relationship revealed a network of areas showing strongest activation for 2/3 power law-consistent trajectories. This network included left dorsal and ventral premotor cortex and IPL, components of the mirror neuron network discussed above, and regions of the temporal-occipital cortex, all areas activated by high amplitude RF trajectories in the Gorbet et al. (2014) study as discussed above. Thus RF trajectories, which are more complex than simple ellipses, yet mathematically tractable in terms of combining simple RF components to form more complex paths, should offer a valuable new stimulus for this very active field of inquiry.

Summary and future research

In summary, RF trajectories provide a motion analogue to the static patterns that have been widely used to examine the limits of global intermediate level shape perception in normal adults (Wilkinson et al., 1998), in the very young (Birch, Swanson, & Wang, 2000), in the elderly (Wang, Morale, Cousins, & Birch, 2009), and in clinical populations (Gallant, Shoup, & Mazer, 2000; Grinter, Maybery, Pellicano, Badcock, & Badcock, 2010; Hess, Wang, Demanins, Wilkinson, & Wilson, 1999; Wang, Wilson, Locke, & Edwards, 2002). We anticipate that the trajectories studied here will provide a similarly useful means of probing the intermediate stages of biological motion analysis. While the present study has extended the parallels between static and trajectory RFs to a much wider

range of frequencies and sizes than our earlier work, it remains to be established to what degree these stimuli tap overlapping or separate neural networks. A fuller examination of threshold performance across the visual field and studies combining the static and motion stimuli to assess their capacity for interference or combination would be valuable next steps.

Keywords: periodic motion trajectories, radial frequency, shape perception, size scaling

Acknowledgments

This work was supported in part by Natural Sciences and Engineering Research Council of Canada (NSERC) Discovery Grants 7551 to FEW and 227224 to HRW. AG was supported as an undergraduate summer trainee by NSERC Collaborative Research and Training Experience (CREATE) Program in Vision Science and Applications (PI: HRW). CCFO was supported by the Postdoctoral Researcher Fellowship from the National Fund for Scientific Research (F.R.S.-FNRS, Belgium).

Commercial relationships: none.
Corresponding author: Frances E. Wilkinson.
Email: franw@yorku.ca.
Address: Centre for Vision Research, York University, Toronto, Ontario, Canada.

References

Achtman, R. L., Hess, R. F., & Wang, Y. Z. (2000). Regional sensitivity for shape discrimination. *Spatial Vision*, *13*(4), 377–391.

Bell, J., & Badcock, D. R. (2009). Narrow-band radial frequency shape channels revealed by sub-threshold summation. *Vision Research*, *49*(8), 843–850, doi:10.1016/j.visres.2009.03.001.

Bell, J., Badcock, D. R., Wilson, H., & Wilkinson, F. (2007). Detection of shape in radial frequency contours: Independence of local and global form information. *Vision Research*, *47*(11), 1518–1522, doi:10.1016/j.visres.2007.01.006.

Bell, J., Wilkinson, F., Wilson, H. R., Loffler, G., & Badcock, D. R. (2009). Radial frequency adaptation reveals interacting contour shape channels. *Vision Research*, *49*(18), 2306–2317, doi:10.1016/j.visres.2009.06.022.

Bidet-Ildeil, C., Orliaguet, J. P., Sokolov, A. N., & Pavlova, M. (2006). Perception of elliptic biological motion. *Perception*, *35*(8), 1137–1147, doi:10.1068/p5482.

Birch, E. E., Swanson, W. H., & Wang, Y. Z. (2000). Infant hyperacuity for radial deformation. *Investigative Ophthalmology and Visual Science*, *41*, 3410–3414. [PubMed] [Article]

Blake, R., & Shiffrar, M. (2007). Perception of human motion. *Annual Review of Psychology*, *58*, 47–73, doi:10.1146/annurev.psych.57.102904.190152.

Brainard, D. H. (1997). The Psychophysics Toolbox. *Spatial Vision*, *10*(4), 433–436.

Daar, M., Or, C. C.-F., & Wilson, H. R. (2012). Increment thresholds for radial frequency trajectories produce a dipper function. *Vision Research*, *73*, 46–52, doi:10.1016/j.visres.2012.09.010.

Danckert, J., & Goodale, M. A. (2001). Superior performance for visually guided pointing in the lower visual field. *Experimental Brain Research*, *137*(3–4), 303–308.

Dayan, E., Casile, A., Levit-Binnun, N., Giese, M. A., Hendler, T., & Flash, T. (2007). Neural representations of kinematic laws of motion: Evidence for action-perception coupling. *Proceedings of the National Academy of Sciences, USA*, *104*(51), 20582–20587, doi:10.1073/pnas.0710033104.

Dumoulin, S. O., & Hess, R. F. (2007). Cortical specialization for concentric shape processing. *Vision Research*, *47*(12), 1608–1613, doi:10.1016/j.visres.2007.01.031.

Gallant, J. L., Braun, J., & Van Essen, D. C. (1993). Selectivity for polar, hyperbolic, and Cartesian gratings in macaque visual cortex. *Science*, *259*(5091), 100–103.

Gallant, J. L., Connor, C. E., Rakshit, S., Lewis, J. W., & Van Essen, D. C. (1996). Neural responses to polar, hyperbolic, and Cartesian gratings in area V4 of the macaque monkey. *Journal of Neurophysiology*, *76*(4), 2718–2739.

Gallant, J. L., Shoup, R. E., & Mazer, J. A. (2000). A human extrastriate area functionally homologous to macaque V4. *Neuron*, *27*(2), 227–235.

Geisler, W. S. (1999). Motion streaks provide a spatial code for motion direction. *Nature*, *400*(6739), 65–69, doi:10.1038/21886.

Geisler, W. S., Albrecht, D. G., Crane, A. M., & Stern, L. (2001). Motion direction signals in the primary visual cortex of cat and monkey. *Visual Neuroscience*, *18*(4), 501–516.

Gorbet, D. J., Wilkinson, F., & Wilson, H. R. (2012). An fMRI examination of the neural processing of periodic motion trajectories. *Journal of Vision*,

12(11):5, 1–15, doi:10.1167/12.11.5. [PubMed] [Article]

Gorbet, D. J., Wilkinson, F., & Wilson, H. R. (2014). Neural correlates of radial frequency trajectory perception in the human brain. *Journal of Vision*, *14*(1):11, 1–19, doi:10.1167/14.1.11. [PubMed] [Article]

Gottwald, V. M., Lawrence, G. P., Hayes, A. E., & Khan, M. A. (2015). Representational momentum reveals visual anticipation differences in the upper and lower visual fields. *Experimental Brain Research*, *233*(8), 2249–2256, doi:10.1007/s00221-015-4294-9.

Grill-Spector, K., Kourtzi, Z., & Kanwisher, N. (2001). The lateral occipital complex and its role in object recognition. *Vision Research*, *41*, 1409–1422.

Grinter, E. J., Maybery, M. T., Pellicano, E., Badcock, J. C., & Badcock, D. R. (2010). Perception of shapes targeting local and global processes in autism spectrum disorders. *Journal of Child Psychology and Psychiatry and Allied Disciplines*, *51*(6), 717–724, doi:10.1111/j.1469-7610.2009.02203.x.

Grossman, E. D., & Blake, R. (2002). Brain areas active during visual perception of biological motion. *Neuron*, *35*(6), 1167–1175.

Habak, C., Wilkinson, F., & Wilson, H. R. (2006). Dynamics of shape interaction in human vision. *Vision Research*, *46*(26), 4305–4320, doi:10.1016/j.visres.2006.08.004.

Habak, C., Wilkinson, F., Zakher, B., & Wilson, H. R. (2004). Curvature population coding for complex shapes in human vision. *Vision Research*, *44*(24), 2815–2823, doi:10.1016/j.visres.2004.06.019.

Hess, R. F., Wang, Y. Z., & Dakin, S. C. (1999). Are judgements of circularity local or global? *Vision Research*, *39*(26), 4354–4360.

Hess, R. F., Wang, Y. Z., Demanins, R., Wilkinson, F., & Wilson, H. R. (1999). A deficit in strabismic amblyopia for global shape detection. *Vision Research*, *39*(5), 901–914.

Jastorff, J., Begliomini, C., Fabbri-Destro, M., Rizzolatti, G., & Orban, G. A. (2010). Coding observed motor acts: Different organizational principles in the parietal and premotor cortex of humans. *Journal of Neurophysiology*, *104*(1), 128–140, doi:10.1152/jn.00254.2010.

Jeffrey, B. G., Wang, Y. Z., & Birch, E. E. (2002). Circular contour frequency in shape discrimination. *Vision Research*, *42*(25), 2773–2779.

Johansson, G. (1973). Visual perception of biological motion and a model for its analysis. *Perception & Psychophysics*, *14*(2), 201–211, doi:10.3758/BF03212378.

Jolicoeur, P., & Ingleton, M. (1991). Size invariance in curve tracing. *Memory and Cognition*, *19*(1), 21–36.

Karim, A. K., & Kojima, H. (2010). The what and why of perceptual asymmetries in the visual domain. *Advances in Cognitive Psychology*, *6*, 103–115.

Khan, M. A., & Lawrence, G. P. (2005). Differences in visuomotor control between the upper and lower visual fields. *Experimental Brain Research*, *164*(3), 395–398, doi:10.1007/s00221-005-2325-7.

Kourtzi, Z., & Kanwisher, N. (2000). Cortical regions involved in perceiving object shape. *Journal of Neuroscience*, *20*(9), 3310–3318.

Kourtzi, Z., Krekelberg, B., & van Wezel, R. J. (2008). Linking form and motion in the primate brain. *Trends in Cognitive Sciences*, *12*(6), 230–236, doi:10.1016/j.tics.2008.02.013.

Lacquaniti, F., Terzuolo, C., & Viviani, P. (1983). The law relating the kinematic and figural aspects of drawing movements. *Acta Psychologica*, *54*(1–3), 115–130.

Lestou, V., Lam, J. M., Humphreys, K., Kourtzi, Z., & Humphreys, G. W. (2014). A dorsal visual route necessary for global form perception: Evidence from neuropsychological fMRI. *Journal of Cognitive Neuroscience*, *26*(3), 621–634, doi:10.1162/jocn_a_00489.

Lestou, V., Pollick, F. E., & Kourtzi, Z. (2008). Neural substrates for action understanding at different description levels in the human brain. *Journal of Cognitive Neuroscience*, *20*(2), 324–341, doi:10.1162/jocn.2008.20021.

Levit-Binnun, N., Schechtman, E., & Flash, T. (2006). On the similarities between the perception and production of elliptical trajectories. *Experimental Brain Research*, *172*(4), 533–555, doi:10.1007/s00221-006-0355-4.

Loffler, G., Wilson, H. R., & Wilkinson, F. (2003). Local and global contributions to shape discrimination. *Vision Research*, *43*(5), 519–530.

Murray, S. O., Olshausen, B. A., & Woods, D. L. (2003). Processing shape, motion and three-dimensional shape-from-motion in the human cortex. *Cerebral Cortex*, *13*(5), 508–516.

Nachmias, J., & Sansbury, R. V. (1974). Grating contrast: Discrimination may be better than detection. *Vision Research*, *14*(10), 1039–1042.

Or, C. C.-F., Khuu, S. K., & Hayes, A. (2007). The role of luminance contrast in the detection of global structure in static and dynamic, same- and oppo-

site-polarity, Glass patterns. *Vision Research*, *47*(2), 253–259, doi:10.1016/j.visres.2006.10.010.

Or, C. C.-F., Khuu, S. K., & Hayes, A. (2010). Moving Glass patterns: Asymmetric interaction between motion and form. *Perception*, *39*(4), 447–463, doi:10.1068/p5917.

Or, C. C.-F., Thabet, M., Wilkinson, F., & Wilson, H. R. (2011). Discrimination and identification of periodic motion trajectories. *Journal of Vision*, *11*(8):7, 1–11, doi:10.1167/11.8.7. [PubMed] [Article]

Oram, M. W., & Perrett, D. I. (1994). Responses of anterior superior temporal polysensory (STPa) neurons to "biological motion" stimuli. *Journal of Cognitive Neuroscience*, *6*(2), 99–116, doi:10.1162/jocn.1994.6.2.99.

Poirier, F. J., & Wilson, H. R. (2006). A biologically plausible model of human radial frequency perception. *Vision Research*, *46*(15), 2443–2455. doi:10.1016/j.visres.2006.01.026

Quick, R. F., Jr. (1974). A vector-magnitude model of contrast detection. *Kybernetik*, *16*(2), 65–67.

Rizzolatti, G., Fadiga, L., Matelli, M., Bettinardi, V., Paulesu, E., Perani, D., & Fazio, F. (1996). Localization of grasp representations in humans by PET: 1. Observation versus execution. *Experimental Brain Research*, *111*(2), 246–252.

Rizzolatti, G., & Sinigaglia, C. (2010). The functional role of the parieto-frontal mirror circuit: Interpretations and misinterpretations. *Nature Reviews: Neuroscience*, *11*(4), 264–274, doi:10.1038/nrn2805.

Schmidtmann, G., Logan, A. J., Kennedy, G. J., Gordon, G. E., & Loffler, G. (2015). Distinct lower visual field preference for object shape. *Journal of Vision*, *15*(5):18, 1–15, doi:10.1167/15.5.18. [PubMed] [Article]

Vinberg, J., & Grill-Spector, K. (2008). Representation of shapes, edges, and surfaces across multiple cues in the human visual cortex. *Journal of Neurophysiology*, *99*(3), 1380–1393, doi:10.1152/jn.01223.2007.

Viviani, P., & Stucchi, N. (1989). The effect of movement velocity on form perception: Geometric illusions in dynamic displays. *Perception and Psychophysics*, *46*(3), 266–274.

Viviani, P., & Terzuolo, C. (1982). Trajectory determines movement dynamics. *Neuroscience*, *7*(2), 431–437.

Wang, Y. Z., Morale, S. E., Cousins, R., & Birch, E. E. (2009). Course of development of global hyperacuity over lifespan. *Optometry and Vision Science*, *86*(6), 695–700, doi:10.1097/OPX.0b013e3181a7b0ff.

Wang, Y. Z., Wilson, E., Locke, K. G., & Edwards, A. O. (2002). Shape discrimination in age-related macular degeneration. *Investigative Ophthalmology and Visual Science*, *43*(6), 2055–2062. [PubMed] [Article]

Weibull, W. (1951). A statistical distribution function of wide applicability. *Journal of Applied Mechanics-Transactions of the ASME*, *18*(3), 293–297.

Westheimer, G. (1979). The spatial sense of the eye. Proctor lecture. *Investigative Ophthalmology and Visual Science*, *18*(9), 893–912. [PubMed] [Article]

Wilkinson, F., Habak, C., & Wilson, H. R. (1997). Peripheral discrimination of quasi-circular forms. *Investigative Ophthalmology & Vision Science*, *38*, S999.

Wilkinson, F., James, T. W., Wilson, H. R., Gati, J. S., Menon, R. S., & Goodale, M. A. (2000). An fMRI study of the selective activation of human extrastriate form vision areas by radial and concentric gratings. *Current Biology*, *10*(22), 1455–1458.

Wilkinson, F., Wilson, H. R., & Habak, C. (1998). Detection and recognition of radial frequency patterns. *Vision Research*, *38*(22), 3555–3568.

Wilson, H. R., & Fung, J. (2016). Effect of motion discontinuities on discrimination of periodic trajectories. *Journal of Vision*, *16*(3):24, 1–8, doi:10.1167/16.3.24. [PubMed] [Article]

Wilson, H. R., & Wilkinson, F. (2002). Symmetry perception: A novel approach for biological shapes. *Vision Research*, *42*(5), 589–597.

Wilson, H. R., & Wilkinson, F. (2014). Configural pooling in the ventral pathway. In J. S. W. L. Chalupa (Ed.), *The new visual neurosciences* (pp. 617–626). Cambridge, MA: MIT Press.

Wilson, H. R., & Wilkinson, F. (2015). From orientations to objects: Configural processing in the ventral stream. *Journal of Vision*, *15*(7):4, 1–10, doi:10.1167/15.7.4. [PubMed] [Article]